Quantum Ratchet Effect for Vortices

J. B. Majer, J. Peguiron, M. Grifoni, M. Tusveld, and J. E. Mooij
Department of Nanoscience, Delft University of Technology, Lorentzweg 1, 2628 CJ Delft, The Netherlands
(Received 23 July 2002; published 4 February 2003)

We have measured a quantum ratchet effect for vortices moving in a quasi-one-dimensional Josephson junction array. In this solid-state device the shape of the vortex potential energy, and consequently the band structure, can be accurately designed. This band structure determines the presence or absence of the quantum ratchet effect. In particular, asymmetric structures possessing only one band below the barrier do not exhibit current rectification at low temperatures and bias currents. The quantum nature of transport is also revealed in a universal/nonuniversal power-law dependence of the measured voltage-current characteristics for samples without/with rectification.

DOI: 10.1103/PhysRevLett.90.056802 PACS numbers: 73.63.–b, 05.40.–a, 74.50.+r, 85.25.–j

A ratchet, i.e., an asymmetric periodic structure, yields the possibility to extract net particle flow from unbiased driving [1]. The last twenty years have seen a great amount of activity aimed at the theoretical understanding of the role of classical fluctuations on the rectification mechanism. Many experimental demonstrations of the classical ratchet effect have been reported ranging from physical to biological systems [2]. In particular, solid-state semiconducting [3] and superconducting devices [4,5] allow for a controlled design. In contrast, the understanding of the role of quantum noise is still at its infancy. On the one hand, the task of describing the interplay among quantum fluctuations, unbiased driving, and spatial potential asymmetry is formidable. The qualitatively new character of quantum ratchets was first pointed out in [6]. Current rectification and reversals in ac-driven ratchet potentials were investigated only recently [7,8]. On the other hand, the lack of experimental realizations of quantum ratchets lies in the difficulty of fabrication of micro- or nanosized structures with controlled asymmetry. Rectification of quantum fluctuations has so far been reported only in triangularly shaped semiconductor heterostructures [9]. Here a current reversal with decrease of temperature was observed as predicted in [6].

In this Letter, we report on the experimental observation of the quantum ratchet effect for vortices moving in quasi-one-dimensional Josephson junction arrays. Those arrays consist of a long, narrow network of Josephson junctions arranged in a rectangular lattice (Figs. 1 and 2). A scanning electron microscope (SEM) picture of part of the most asymmetric mesoscopic device is shown in Fig. 1.

The potential shape felt by the vortices along the longitudinal direction can be accurately designed by properly choosing the junction sizes and/or the interjunction distances. A quantum ratchet effect is observed in an asymmetric array providing a ratchet potential with three bands below the barrier. Strikingly, current rectification is *absent* in asymmetric arrays supporting only one band at low enough temperatures and bias currents. This is a consequence of time-reversal symmetry combined with translational properties of a one-band ratchet potential. In the following we introduce the basic properties of quasi-one-dimensional Josephson junction arrays [10]. Subsequently, we show how a ratchet potential for vortices can be designed. We finally report on the experimental results and their interpretation.

Our arrays consist of a network of rectangular superconducting islands, each weakly coupled to its four neighboring islands by Josephson junctions. Applying a magnetic field perpendicular to the array induces vortices in the system. The vortex density is proportional to the magnetic field strength [10]. To confine the vortex

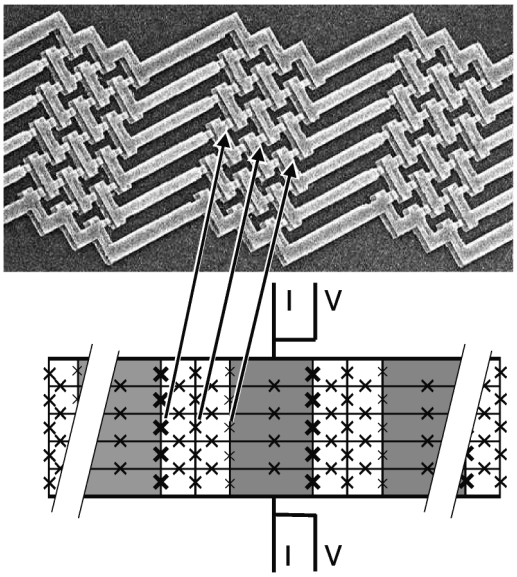

FIG. 1. Strongly asymmetric array that exhibits ratchet effects. Top: scanning electron microscope picture. Bottom: schematic layout. Josephson junctions are represented by a cross, cells are areas enclosed by four junctions. All measured arrays have a length of 303 cells and a width of 5 cells between solid superconducting electrodes (busbars). Vortices are induced by an applied magnetic field perpendicular to the array. Cells areas are 2.8 μm^2 (gray) and 0.7 μm^2 (white). Junctions indicated by arrows have areas of 240×100 nm^2, 200×100 nm^2, and 160×100 nm^2, respectively. Vortices have lower energy in cells with larger area and smaller junctions.

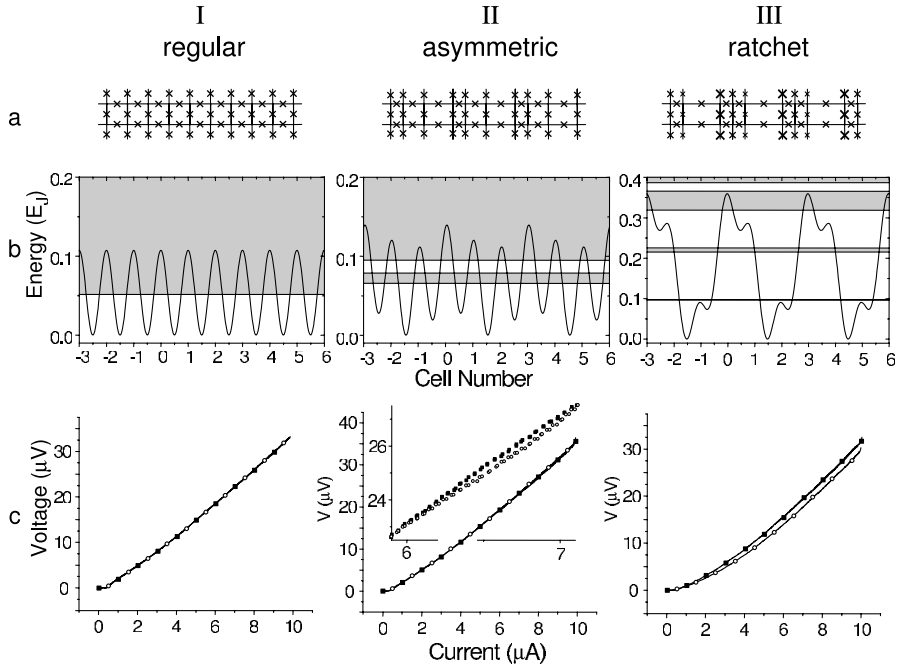

FIG. 2. Samples and measurement results. The top row (a) indicates three supercells for each of the three arrays, row (b) the resulting potential and the calculated vortex bands. Sample I has a cosine-shaped potential with one energy band that connects with a continuum. Sample II shows a weak asymmetric potential with one band below the continuum. Sample III has a strongly asymmetric potential with three energy bands below the continuum. The bottom row (c) gives the results for voltage (vortex current) versus bias current (vortex force), measured at 12 mK and a density s of 0.61 vortices per supercell. Open circles label the positive branch and closed squares the negative branch. Sample III shows a clear asymmetry. Sample II shows a weak asymmetry only at high bias as seen in the inset.

motion in one dimension, superconducting strips (called busbars, cf. Fig. 1) are applied along the two long edges of the array. The superconducting current and voltage electrodes along the length of the array repel the vortices, which consequently are forced to move along the center row. When the vortices move, they create a voltage $V = sv\Phi_0/a$ across the array, which is measured at the end of the busbars. Here s is the one-dimensional vortex density, a is the average junction distance in the longitudinal direction, and $\Phi_0 = h/2e$ is the superconducting flux quantum. Finally, v is the average vortex velocity, and is influenced by all the microscopic details of the vortex dynamics. At low vortex densities, vortex-vortex interactions can be neglected [11], and the dynamics of a single vortex is homologous to that of a mass-carrying particle in a one-dimensional periodic potential [12]. For a regular array the potential is approximately cosine shaped [13] [see Fig. 2(b) left].

The amplitude of the potential variation is proportional to the Josephson coupling energy $E_J = I_c\Phi_0/2\pi$, with I_c the critical current of a single junction. By varying the cell areas or the junction sizes the potential can be modified. Increasing the cell area increases the magnetic flux in the cell for a given magnetic field, which results in a lowering of the potential minimum. Modifying the junction size changes the Josephson energy and the height of the barrier for vortex motion between cells. These two methods allow for a tailored design of the potential, such as strength and symmetry. The mass of the vortex is proportional to the average capacitance C of the junctions, $m_v \approx \Phi_0 2C/2a^2$ [12,13]. The great advantage of a Josephson junction array is that both parameters, the potential E_J and the mass m_v, can be controlled by fabrication parameters. Damping is included phenomenologically upon introducing a friction term $-\eta v$ in the equations of motion. Within a resistively shunted junction (RSJ) model the viscosity of a regular array is estimated to be $\eta = \Phi_0^2/2a^2 r_e$ [12], with $r_e = 1.5\,\mathrm{k}\Omega$ being the estimated normal state resistance of the junctions. Finally, vortices are put into motion upon injecting a current I into the busbars, which exerts a Lorentz-like force on such particles. Such force is $F = I\Phi_0/N_c a$, where $N_c = 304$ is the chosen number of junction columns in the array.

At low temperatures, tunneling processes through the barrier become relevant for a vortex of low mass and a weak pinning potential [14,15]. In the junction arrays that we have designed the quantum regime is reached when the charging energy $E_c = e^2/2C$ is of the order of the amplitude of the potential, and for low enough temperatures. In this regime, the quantum vortex is able to tunnel, interfere, or to localize [14,15]. The degree of quantum coherence in the motion of a vortex is strongly dependent on the amount of dissipation. As a minimal model to describe the dissipative quantum dynamics of a single vortex, we consider the system-plus-bath Hamiltonian [16] $\hat{H}_{\mathrm{tot}}(t) = \hat{H}_{\mathrm{R}} + \hat{x}F(t) + \hat{x}\hat{\xi}(t) + \hat{H}_{\mathrm{B}}$. Here

$$\hat{H}_{\mathrm{R}} = \hat{p}^2/(2m_v) + V_{\mathrm{R}}(\hat{x}) \qquad (1)$$

is the isolated ratchet Hamiltonian for a vortex of mass m_v moving in the periodic potential $V_{\mathrm{R}}(x + L) = V_{\mathrm{R}}(x)$. The action of the deterministic force is in the interaction term $\hat{x}F(t)$. Finally, $\hat{x}\hat{\xi} + \hat{H}_{\mathrm{B}}$ is the standard Hamiltonian of an ensemble of harmonic oscillators bilinearly coupled to the vortex via the collective force operator $\hat{\xi}$. The character of the bosonic bath is then fully captured by the spectral function $J(\omega) = \eta\omega$, being related to the Fourier transform of the force-force correlator $\langle\hat{\xi}(t)\hat{\xi}(s)\rangle$.

We have designed, fabricated, and investigated three arrays with identical average properties (Fig. 2). Two of them (samples II and III) are superlattices, where a sequence of three cells is repeated along the length of the array. We refer to this set of three cells as the supercell with length L. The devices are fabricated from aluminum on a silicon substrate using shadow evaporation techniques. Sample I (regular) is an array with all cell areas equal to $a^2 = 1.4\ \mu\text{m}^2$, and all junction sizes equal to $100 \times 200\ \text{nm}^2$. These junctions have a capacitance C of 2 fF. The critical current I_c of the junctions is 210 nA, which is determined from the normal state resistance using the Ambegaokar-Baratoff relation [17]. The characteristic energy scales are $E_J \approx 10E_c \approx 5\text{K}k_\text{B}$. This regular sample serves as a reference for the other samples; the "supercell" here consists of three identical basic cells. In sample II (weakly asymmetric) the cell size is varied periodically along the length of the array. The areas were chosen as 0.5-1-1.5 relative to the regular sample. The five cells across the width of the array all have the same area. As expected, the resulting potential (Fig. 2(b), center) is asymmetric. The cell areas of the third sample (sample III, strongly asymmetric) were chosen as 0.5-2-0.5 relative to the regular sample, and in addition the width of the vertical junctions varied as 1.2-1-0.8 relative to the reference junction. The resulting potential [Fig. 2(b), right] is strongly asymmetric. The three samples were fabricated on the same substrate under identical conditions. In the presented experiments a dc current was swept between -10 and $10\ \mu$A. We measured the dc voltage across the width of the array as a function of the applied bias current. The ratchet effect manifests itself as a difference between the voltages for positive and negative bias currents. To observe this difference we invert the negative branch of the current-voltage curve with respect to the origin [Fig. 2(c)]. Measurements were carried out in a dilution refrigerator between 12 mK and 1 K.

The measurements at 12 mK show a clear ratchet effect for the strongly asymmetric sample. However, no voltage asymmetry is observed between positive and negative current drives for the regular sample and for the weakly asymmetric sample at low bias currents. The symmetry for the regular array serves as a check for the validity of the experimental methods. The lack of voltage asymmetry for sample II at low currents is remarkable, however. This can be understood by observing that the ratchet Hamiltonian for sample II has only one energy band that is well separated by a gap from the continuum at higher energies [Fig. 2(b), center)]. Because of the low temperature (12 mK $= 0.0024\ E_J$), only the low lying energy band $\mathcal{E}_1(k)$ is occupied. As we now show, despite the asymmetry, a single band ratchet Hamiltonian supports no current rectification.

The energy bands of a generic isolated ratchet Hamiltonian, Eq. (1), are obtained by solving the Schrödinger equation $\hat{H}_\text{R}|n, k\rangle = \mathcal{E}_n(k)|n, k\rangle$ (n band index, k wave vector). Time-reversal symmetry and the periodicity of the potential imply $\mathcal{E}_n(k) = E_n + \sum_{m=1}^{\infty}[\Delta_n^{(m)}/2]\cos(mkL)$. To know wether a single band asymmetric Hamiltonian supports a ratchet effect, we restrict to the lowest band $n = 1$ of the potential, and express $\hat{H}_\text{R}$ in the basis which diagonalizes the discrete position operator $\hat{x} = \sum_{M=-\infty}^{\infty} ML|M\rangle\langle M|$ (so termed discrete variable representation, DVR, [18,19]). $|M\rangle$ describes a state which is localized at cell M. We observe that the driving and noise terms, $\hat{x}F$ and $\hat{x}\hat{\xi}$, are already diagonal in this basis. Then the one-band Hamiltonian assumes the expression

$$\hat{H}_\text{R} = \sum_{M=-\infty}^{\infty}\Bigg[E_1|M\rangle\langle M| + \sum_{m=1}^{\infty}\frac{\Delta_1^{(m)}}{4}(|M\rangle\langle M+m| + |M+m\rangle\langle M|)\Bigg]. \tag{2}$$

Note that the same form holds for a symmetric periodic potential. In fact a change $\hat{x} \to -\hat{x}$ leaves $\hat{H}_\text{R}$ invariant, and no ratchet effect occurs. The situation is different when more than one band contributes to transport. In sample II this occurs at large enough bias currents (inset Fig. 2(c)) or temperatures (Fig. 4). In Ref. [8] a detailed theory on the role of the higher bands has been developed for few bands ac-driven quantum ratchets. This theory can also be adapted to describe the behavior of sample III in the region of moderate dc-bias currents ($FL \leq U_0$, with U_0 the potential barrier), such that Wannier-Stark states generated by the bands lying above the barrier are not relevant. A theory capable of describing the strong current regime is presently not available, and is the object of current research. In general, when dissipative transitions between different energy bands occur, the total forward/backward rates reflect the intrawell (vibrational motion) as well as the interwell (tunneling) dynamics. The breaking of detailed balance symmetry between backward

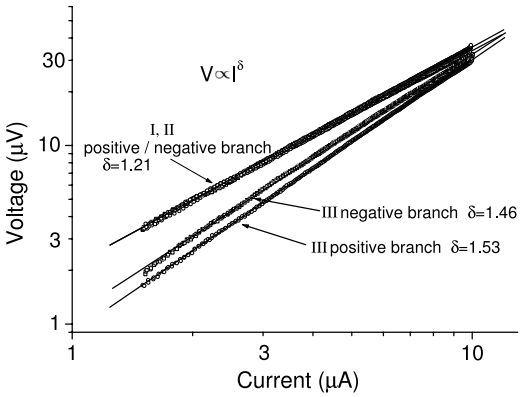

FIG. 3. Power-law dependence of the V-I characteristics at 12 mK. All the three samples exhibit above 1.5 μA a behavior $V \propto I^\delta$, $\delta > 1$. Because three energy bands are involved in the dynamics, sample III shows a a larger power than samples I and II. The classical behavior would correspond to linear V-I characteristics, i.e., $V \propto I$.

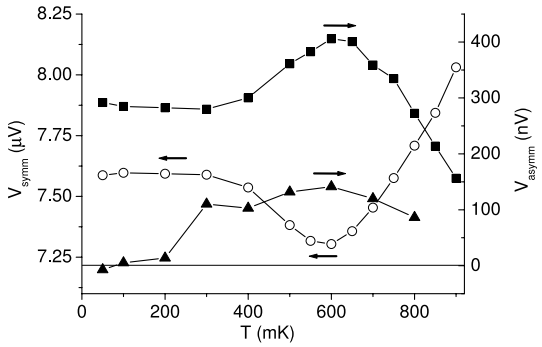

FIG. 4. Temperature dependence of the ratchet effect. Plotted with closed symbols on the right scale (squares sample III, triangles sample II): V_{asymm} defined as the difference between the voltages for negative and positive currents. Plotted with open symbols (only sample III) on the left scale: V_{symm} defined as the mean of these voltages. The bias current is 6 μA for sample III, and 4 μA for sample II.

and forward rates then implies a ratchet effect, i.e., $V(F) \neq -V(-F)$.

Another signature of quantum behavior is depicted in Fig. 3. For a classical dynamics and zero temperature $V \propto I$ is expected above the critical current. However, all of the three samples exhibit a power-law behavior $V \propto I^{\delta}$ with exponent $\delta > 1$ for moderate-to-large currents. Strikingly, for a large range of currents, samples I and II are lying on top of each other, despite the dissimilarity of the underlying potential. For sample III we measure different powers for the two slopes which are higher than the powers of the previous samples. We find it worthy of notice, however, to observe that a power-law behavior $I \propto F^{2K-1}$, with K the Kondo parameter, is expected to be seen at low temperatures ($k_{\text{B}}T \ll FL$) and moderate bias F such that a tight-binding description is still applicable [16] (it corresponds to bias currents up to about 2 μA). We find it puzzling that at the largest bias currents of the experiments a similar power-law is also observed.

Figure 4 shows the temperature dependence of the ratchet signal. On the right axis the difference V_{asymm} between the two branches is plotted for a fixed bias and density ($s = 0.38$ sample II; $s = 0.28$ sample III). We also include the mean of the two branches V_{symm} (plotted on the left axis) for sample III. Below 350 mK down to the base temperature of 12 mK the signals stay constant for sample III. This is a clear quantum signature. In fact a classical ratchet effect, resulting from thermal activation, should disappear at low temperatures. Above 350 mK the ratchet signal increases up to 650 mK and then decreases for higher temperatures. The decrease above 650 mK is due to the reduction of the Josephson energy that sets in when the critical temperature of the superconductor is approached, in combination with the increase of the thermal energy. Because of the weaker potential the asymmetry becomes less important and the ratchet effect decreases. The fact that the mean transport increases is consistent with that picture. The increase of the ratchet effect in the intermediate regime (350–650 mK) is due to the generation of quasiparticles. These quasiparticles are an additional source of friction and cause the ratchet effect to increase [6]. Because of the additional damping the mean transport is reduced. Similar features are exhibited by sample II.

In summary, the band structure plays an important role for a quantum ratchet. For an asymmetric periodic potential with only one relevant energy band below the barrier the ratchet effect is missing at low temperatures and bias. For a sample with three energy bands we measure a ratchet effect even at low temperatures. Quantum signatures are also a saturation of the signal at low temperatures, and a power-law behavior at moderate-to-high currents. Finally, additional friction increases the ratchet effect.

We thank M. S. Ferreira, P. Hadley, P. Hänggi, C. J. P. M. Harmans, and M. Thorwart for discussions, as well as A. van den Enden and R. Schouten for technical assistance. This work was supported by the Dutch Foundation for Fundamental Research on Matter (FOM).

[1] P. Reimann, Phys. Rep. **361**, 57 (2002).
[2] Special issue on *Ratchets and Brownian Motors: Basics, Experiments and Applications* [Appl. Phys. A **75** (2002)].
[3] A. Lorke *et al.*, Physica (Amsterdam) **249B**, 312 (1998).
[4] F. Falo *et al.*, Appl. Phys. A **75**, 263 (2002).
[5] A. Sterck, S. Weiss, and D. Koelle, Appl. Phys. A **75**, 253 (2002).
[6] P. Reimann, M. Grifoni, and P. Hänggi, Phys. Rev. Lett. **79**, 10 (1997).
[7] S. Scheidl and V. Vinokur, Phys. Rev. B **65**, 195305 (2002).
[8] M. Grifoni, M. S. Ferreira, J. Peguiron, and J. B. Majer, Phys. Rev. Lett. **89**, 146801 (2002).
[9] H. Linke *et al.*, Science **286**, 2314 (1999).
[10] C. Bruder, L. I. Glazman, A. I. Larkin, J. E. Mooij, and A. van Oudenaarden, Phys. Rev. B **59**, 1383 (1999).
[11] In our experiment all voltages depend linearly on the applied magnetic field for average flux up to 0.7 flux quanta per supercell. As the vortex density scales with the flux, this indicates a weak interaction among vortices.
[12] T. P. Orlando, J. E. Mooij, and H. S. J. van der Zant, Phys. Rev. B **43**, 10218 (1991).
[13] C. J. Lobb, D.W. Abraham, and M. Tinkham, Phys. Rev. B **27**, 150 (1983).
[14] A. van Oudenaarden and J. E. Mooij, Phys. Rev. Lett. **77**, 4257 (1996).
[15] A. van Oudenaarden and J. E. Mooij, Phys. Rev. Lett. **76**, 4947 (1996).
[16] U. Weiss, *Quantum Dissipative Systems* (World Scientific, Singapore, 1999), 2nd ed.
[17] V. Ambegaokar and A. Baratoff, Phys. Rev. Lett. **10**, 486 (1963).
[18] M. Thorwart, M. Grifoni, and P. Hänggi, Phys. Rev. Lett. **85**, 860 (2000).
[19] Note that the DVR basis coincides with the Wannier basis only within a tight-binding approximation.